

# Measurement and Defect Detection of the Weld Bead Based on Online Vision Inspection

Yuan Li, *Member, IEEE*, You Fu Li, *Senior Member, IEEE*, Qing Lin Wang, De Xu, *Member, IEEE*, and Min Tan

**Abstract**—Weld bead inspection is important for high-quality welding. This paper summarizes our work on weld bead profile measurement, monitoring, and defect detection using a structured light-based vision inspection system. The configuration of the sensor is described and analyzed. In this configuration, the system presented in this paper can easily be calibrated. The image processing and extraction algorithms for laser profiles and feature points are presented. The dimensional parameters of the weld bead are measured, and the weld defects are detected during multilayer welding processes. Experiments using the vision inspection system were conducted with satisfactory results for online inspection.

**Index Terms**—Flaw detection, inspection, machine vision, visual system, welding.

## I. INTRODUCTION

WELDING is important for the manufacturing industry, particularly in shipbuilding, railway, and pipeline construction industries. Recently, people have begun to explore the use of welding automation to improve both weld bead quality and welding productivity. Although robots with advanced sensors have been implemented for welding automation, they often work in a “teach-and-playback” mode, in which a robot repeatedly follows a preprogrammed path. With the introduction of seam tracking systems, automated welding systems can now follow a real weld seam rather than simply follow a preprogrammed path. However, this does not mitigate the need for postwelding seam inspection, which is critical to ensure high welding quality. Currently, most systems perform weld seam inspection after completing the welding process because they are not capable of online inspection. As a result, finished weldments with defects have to be gas cut and welded again, reducing productivity. Moreover, it is challenging to control the weld bead quality without online weld bead profile monitoring, further degrading the weld system’s performance. Online

inspection provides real-time weld quality information that can be used to optimize welding parameters and reduce cycle time and material wastes by terminating the welding process when weld defects are detected.

Methods of weld bead inspection commonly in use include radiographic inspection, ultrasonic inspection, vision inspection, and magnetic detection. Radiographic inspection is a nondestructive testing method using radiographic sensors and is applicable to most weldment [1], [2]. However, these sensors cannot be installed on weld lines to support online weldment inspection. Ultrasonic inspection, although being widely implemented because of its flexibility and low cost [3], [4], lacks a visual record and requires highly skilled operators to perform defect recognition. Magnetic defect detection has high sensitivity and is easy to operate [5]. However, this method is limited to ferromagnetic materials, and its manual operation is not applicable to automated inspection.

The strengths of vision sensing and computer vision have led to the development of computer-vision-based surface defect detection applications. Examples include circuit board inspection using vision and infrared sensors [6], defect detection on smooth surfaces using optical mechatronic systems [7], and surface defect recognition and classification using vision sensors [8]. Vision sensors are also used to measure weldment distortion [9] and track seams so that other sensors can inspect the quality of the weld bead generated by the welding system [10]. Distance sensors are also used to identify and track the weld seam during inspection [11].

Seam tracking systems have been developed to guide a weld gun along a weld seam to improve weld bead quality. For these systems, online inspection of the weld bead is still needed to guarantee a high quality of welding. In particular, monitoring both the weld bead profile in the groove and weld defects is highly desirable. In previous works, online weld quality estimation systems have been developed to monitor various parameters [12] and to measure the weld fusion state using weld pool images and neurofuzzy models [13]. Some vision-based measurement systems have been developed to perform weldment inspection, alignment, positioning, and seam tracking [14]–[17], although they suffer from illumination variations and heavy specular reflection on smooth weldment surfaces. As a result, a machine vision system using laser-generated structured light is recommended because of its reliability and ability to collect much useful information during welding. The vision measurement principle of laser triangulation and the definition of weld bead dimensions have previously been presented in [14] and [15]. However, a detailed analysis of the imaging model for the vision sensor has not yet been performed, and

Manuscript received June 30, 2008; revised June 11, 2009; accepted June 12, 2009. Date of publication October 16, 2009; date of current version June 9, 2010. This work was supported in part by the National High Technology Research and Development Program of China under Grant 2006AA04Z213, by the National Natural Science Foundation of China under Grant 60725309, and by the Research Grants Council of Hong Kong under Project CityU117507. The Associate Editor coordinating the review process for this paper was Dr. Dario Petri.

Y. Li and Q. L. Wang are with Beijing Institute of Technology, Beijing 100081, China (e-mail: liyuan@compsys.ia.ac.cn; wqlbit@gmail.com).

Y. F. Li is with the City University of Hong Kong, Kowloon, Hong Kong (e-mail: meyfli@cityu.edu.hk).

D. Xu and M. Tan are with the Institute of Automation, Chinese Academy of Sciences, Beijing 100190, China (e-mail: xude@compsys.ia.ac.cn; tan@compsys.ia.ac.cn).

Color versions of one or more of the figures in this paper are available online at <http://ieeexplore.ieee.org>.

Digital Object Identifier 10.1109/TIM.2009.2028222

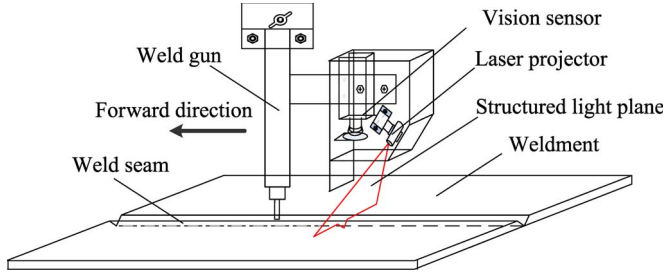


Fig. 1. Sketch of the vision sensor and welding system.

the algorithms for feature extraction and defect detection need to be further explained in detail. The online inspection system studied in this paper was presented in an earlier work [18] by the authors. In this paper, we focus on the key issues in weld bead vision inspection, such as the sensor imaging model, vision measurement, and defect detection. Based on a detailed analysis of the sensor imaging model, a vision inspection system is proposed for monitoring a weld bead profile. Because the system directly operates in the image domain, complicated 3-D measurement procedures, which often lead to inaccurate estimations, are avoided. The inspection system monitors weld bead dimensions to detect defects based on the measurements of groove width, weld bead width, filling depth, reinforcement height, plate displacement, weld bead misalignment, and undercut.

The rest of this paper is organized in the following manner: In Section II, the structure and model of the inspection sensor are described, and the inspection measurement variables are defined. The feature extraction and vision measurement algorithms are presented in Section III. In Section IV, the experimental results of online vision measurement and defect detection for weld bead are presented. This paper is concluded in Section V.

## II. WELD INSPECTION SENSOR

### A. Structure and Configuration of the Sensor

A vision inspection sensor using structured light has been designed to monitor the weld bead profile. A laser emitter projects a structured light plane onto the weldment to form a laser stripe that is captured by a camera with an optical filter. The camera is shielded to protect against arc lights and splashes. The inspection sensor, which is composed of the camera and the laser emitter, is mounted on the back of the weld gun and above the weldment, as shown in Fig. 1. During welding, the inspection sensor scans the surface of the weld bead behind the weld gun to monitor its surface and the filling profile in the weld groove. Weld defects, should there be any, are detected in this process.

Fig. 2 illustrates the pose relationship between the vision sensor and weldment, including the camera reference frame  $\mathcal{C}$ , the weldment reference frame  $\mathcal{W}$ , the structured light plane  $\Pi_1$ , and the weldment surface plane  $\Pi_2$ . In the reference frame  $\mathcal{W}$ , the  $z_w$  axis of  $\mathcal{W}$  corresponds to the unit normal vector of  $\Pi_2$ , and the  $x_w$  axis of  $\mathcal{W}$  corresponds to the forward direction of the weld seam. The camera reference frame  $\mathcal{C}$  is defined as

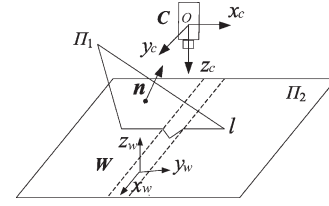


Fig. 2. Frame definition of the vision sensor and weldment.

$x_c = y_w$ ,  $y_c = x_w$ , and  $z_c = -z_w$ . The normal vector  $\mathbf{n}$  of  $\Pi_1$  lies in the plane defined by  $y_c$  and  $z_c$ .

### B. Model of the Inspection Sensor

Vision measurement normally involves tedious calibration and complicated 3-D reconstruction that often lead to inaccurate estimations. In this section, the vision measurement of the inspection sensor is formulated and analyzed. In the configuration of the inspection sensor, the weld dimensions can directly be measured using the coordinates of the pixels.

The imaging property of a camera is described using the pinhole camera model. The intrinsic model of a camera can be written as

$$\begin{bmatrix} u \\ v \\ 1 \end{bmatrix} = \begin{bmatrix} a_x & 0 & u_0 \\ 0 & a_y & v_0 \\ 0 & 0 & 1 \end{bmatrix} \begin{bmatrix} x_c/z_c \\ y_c/z_c \\ 1 \end{bmatrix} \quad (1)$$

where

- $u$  and  $v$  are the coordinates of a point in an image plane;
- $a_x$  and  $a_y$  are the magnification coefficients from the normalized focus image plane coordinates to the image plane coordinates;
- $u_0$  and  $v_0$  are the coordinates of the camera's principal point in the image plane;
- $x_c$ ,  $y_c$ , and  $z_c$  are the coordinates of a point in  $\mathcal{C}$ .

The coordinates of each image point  $[x \ y]^T$  on the normalized focus image plane is calculated as

$$\begin{bmatrix} x \\ y \end{bmatrix} = \frac{1}{z_c} \begin{bmatrix} x_c \\ y_c \end{bmatrix} = \begin{bmatrix} (u - u_0)/a_x \\ (v - v_0)/a_y \end{bmatrix}. \quad (2)$$

The equation of  $\Pi_1$  in  $\mathcal{C}$  is

$$ax_c + by_c + cz_c + 1 = 0 \quad (3)$$

where  $a$ ,  $b$ , and  $c$  are the coefficients of the light plane equation. The structured light plane is projected onto the weldment, where visual features are inferred from deformation of the reflected laser stripe. An arbitrary point  $P$  on the stripe is on the line defined by the optical center of the camera  $O$  and its image point  $[x \ y \ 1]^T$  on the normalized focus image plane. The equation of the line in  $\mathcal{C}$  is given by

$$\begin{bmatrix} x_c \\ y_c \\ z_c \end{bmatrix} = t \begin{bmatrix} x \\ y \\ 1 \end{bmatrix} \quad (4)$$

where  $t$  is the variable parameter of the line. Using (3) and (4), the field depth  $z_c$  can be calculated as

$$z_c = - \left( [a \quad b \quad c] \begin{bmatrix} x \\ y \\ 1 \end{bmatrix} \right)^{-1} \quad (5)$$

which is the constraint condition for the vision measurement based on structured light. The equation of  $\Pi_2$  in  $C$  is

$$Ax_c + By_c + Cz_c + 1 = 0 \quad (6)$$

where  $A$ ,  $B$ , and  $C$  are the coefficients of the weldment surface plane equation.

The laser stripe  $l$  is the intersection of  $\Pi_1$  and  $\Pi_2$ . Combining (2) and (6) with the constraint condition (5), the equation of the stripe  $l$  on the normalized focus image plane is obtained, i.e.,

$$(A - a)x + (B - b)y + C - c = 0. \quad (7)$$

With the configuration of the sensor illustrated in Fig. 2, it can be seen that  $A = 0$  and  $a = 0$  when the sensor is aligned with the weldment. In this case, the stripe  $l$  is parallel to the  $x_c$  axis in  $C$ , as indicated by (7). Thus, the weld bead variables along the  $y$ -axis of the weldment are proportional to the pixel coordinates on the stripe and can be evaluated by the following coordinates:

$$dx_c = k_u du \quad (8)$$

where  $d$  represents the derivative, and  $k_u$  is a scalar factor.

The relationship between the derivatives of the point coordinates in  $C$  and in the image space is [16]

$$\begin{bmatrix} dx_c \\ dy_c \\ dz_c \end{bmatrix} = z_c^2 \begin{bmatrix} -\frac{b}{a_x a_y} (v - v_0) - \frac{c}{a_x} & -\frac{b}{a_x a_y} (u - u_0) \\ \frac{a}{a_x a_y} (v - v_0) & -\frac{a}{a_x a_y} (u - u_0) - \frac{c}{a_y} \\ \frac{a}{a_x} & \frac{b}{a_y} \end{bmatrix} \begin{bmatrix} du \\ dv \end{bmatrix}. \quad (9)$$

We can substitute  $a = 0$  into (9) to generate the coordinates of the point in the camera frame. This takes the form

$$dz_c = z_c^2 \frac{b}{a_y} dv = k_v dv \quad (10)$$

where  $dz_c$  and  $dv$  are the derivatives of the pixel coordinates in  $C$  and in an image, and  $k_v$  is a scalar factor. The variables  $k_u$  and  $k_v$  are constants when the sensor is aligned with the weldment. They can be calculated using the pixel coordinates of the feature points in an image and the dimensions of a weldment, according to (8) and (10). Thus, the scale of the vision system can easily be in-field calibrated using a ruler. The weld bead is measured with respect to the visual feature of each stripe, which eliminates the need for tedious calibration and complicated 3-D reconstruction.

As illustrated in Fig. 3, the distance  $d'$  on the image plane is approximately proportional to the depth variable  $d$  when the distance to the surface is much greater than the focal length of the camera. This fact graphically illustrates the relationship represented by (10) and can be explained using the weak perspective projection model.

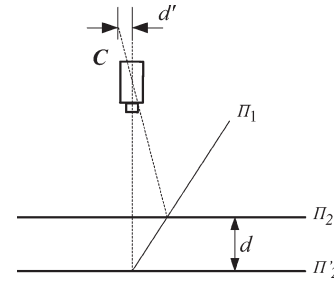


Fig. 3. Vision measurement principle of laser triangulation. The variable in the field depth is approximately proportional to an offset in the image plane.

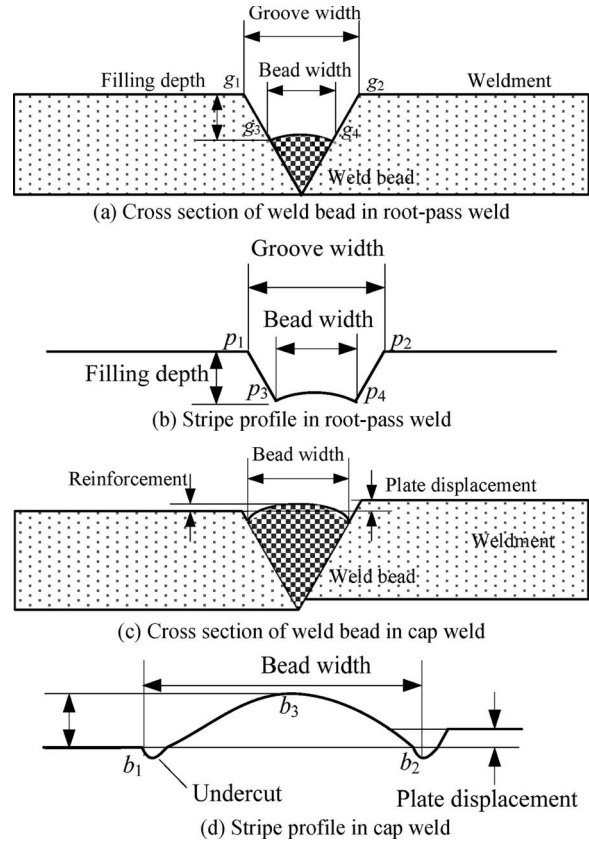


Fig. 4. Definition of weld bead dimensions in multilayer weld. (a) Cross section of the weld bead in root-pass weld. (b) Stripe profile in root-pass weld. (c) Cross section of the weld bead in cap weld. (d) Stripe profile in cap weld.

### C. Inspection Contents

The vision inspection system generates the dimensions and the surface parameters of the weld bead (e.g., the bead width, filling depth, and weld reinforcement height). Some of these variables can identify the weld defects (e.g., the bead misalignment, displacement of weldment, and undercut). Fig. 4 illustrates the terms and variables used when referring to root-pass and cap stages of the welding process.

## III. FEATURE EXTRACTION AND VISION MEASUREMENT

The dimensions of the weld bead are measured using feature points in weld images. In this section, the algorithms for extracting the laser profile and the weld bead feature points are explained. The detection criterions for several weld defects are also presented.

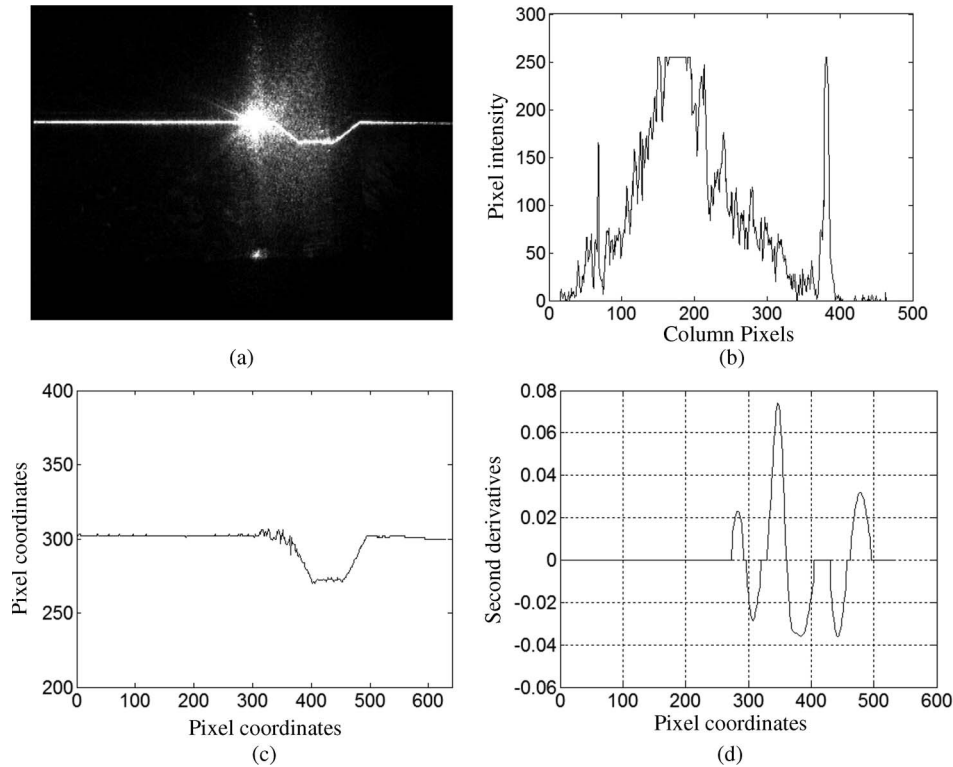


Fig. 5. Profile extraction of laser stripes. (a) Original image. (b) Typical intensity distribution of column pixels. (c) Extracted profile. (d) Second derivative of the profile in (c).

#### A. Profile Extraction of Laser Stripes

Image processing is simplified by using structured light. There are, however, still problems to address, including false imaging, confusion caused by strong reflections from smooth surfaces, and splashes during welding. Some algorithms have been developed for image processing and stripe profile extraction based on intensity distribution, such as maximum searching, center of gravity, intensity distribution fitting, and multipeak detection [19]. To improve the robustness of stripe profile extraction, a method for feature extraction was developed for the initial stage and during the welding and is presented here.

In the initial stage of welding, because there are no arc light or splash disturbances in the weld images, the extraction algorithm using intensity distribution and continuity constraints can reliably extract the stripe profile. First, the stripe figure in the images is detected by a quick intensity search of pixels. Points on each stripe are extracted column by column based on the intensity distribution of column pixels. Those points caused by false imaging are rejected using temporal and spatial continuity constraints. Finally, the stripe profile is obtained using linear interpolation and Gaussian filtering.

During welding, weld images are corrupted with arc lights and weld splashes. To minimize the effect of these disturbances, the images are preprocessed before the profile is extracted. The stripe features remain stable while the intensities of splashes rapidly and acutely change in weld images. Thus, an image operation is used to eliminate the splashes. This operation involves taking the smallest intensity of the corresponding pixels in a sequence of consecutive images. This way, weld images are segmented using an adaptive threshold to filter out variable illumination by arc lights.

#### B. Feature Extraction and Dimension Measurement

Visual features are used for measurement and defect detection of the weld bead. In this section, we present the algorithms for feature extraction for both root-pass weld and cap weld. For the former, the filling state in the weld groove is investigated, and for the latter, we focus on the quality of the weld bead. Weld defects are detected during the welding process.

The turning points  $p_1$ ,  $p_2$ ,  $p_3$ , and  $p_4$  on the laser stripe profile correspond to the brim points  $g_1$ ,  $g_2$ ,  $g_3$ , and  $g_4$  in the weld groove, as shown in Fig. 4(a) and (b). The turning points are selected as the feature points for monitoring the filling profile in the weld groove during root-pass weld. The turning points in the stripe profile display extreme curvature. The feature points can be located by calculating the second derivative of the stripe profile and extracting  $p_1$ ,  $p_2$ ,  $p_3$ , and  $p_4$  as the local maximum and minimum values.

The feature extraction algorithm is performed in the following manner: First, the baseline of the stripes on the surface of weldment is detected using a Hough transform. Then, the second derivative of the stripe profiles is calculated. The noise in the signal introduces additional curvature extrema into the stripe profile that appear as local minima and maxima in the second derivative of the stripe profile. The four feature points are extracted by the absolute value of the extremum. Then, the dimensions of the weld bead are calculated from the coordinates of the visual feature points  $p_{1u}$ ,  $p_{1v}$ ,  $p_{2u}$ ,  $p_{2v}$ ,  $p_{3u}$ ,  $p_{3v}$ ,  $p_{4u}$ , and  $p_{4v}$ , as shown in the list that follows.

- 1) The width of the weld groove  $W_g$  is obtained by

$$W_g = k_u(p_{2u} - p_{1u}).$$

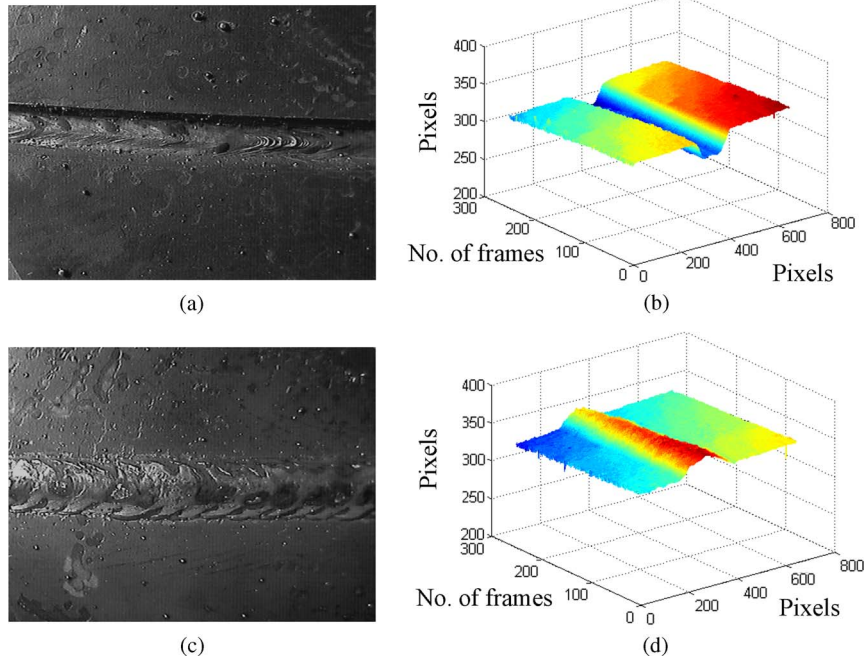


Fig. 6. Photos and profiles of the weld beads in defect-free multilayer weld. (a) and (c) Photos of the weld bead. (b) Profiles of a defect-free weld bead in root-pass weld. (d) Profiles of a defect-free weld bead in cap weld.

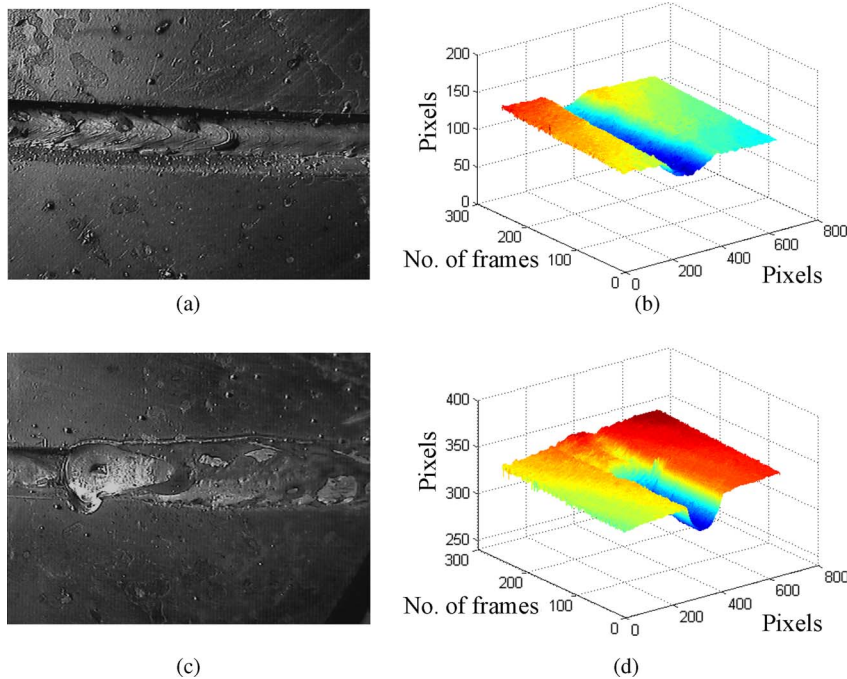


Fig. 7. Photos and profiles of the weld beads in multilayer weld with defects. (a) and (c) Photos of the weld beads. (b) Profiles of a weld bead with a misalignment defect in root-pass weld. (d) Profiles of a weld bead with an undercut defect in cap weld.

2) The width of the weld bead  $W_b$  is obtained by

$$W_b = k_u(p_{4u} - p_{3u}).$$

3) The filling depth of the weld groove  $D_f$  is obtained by

$$D_f = k_v [(p_{3v} + p_{4v}) - (p_{1v} + p_{2v})] / 2.$$

For cap welding, the variables of interest are the weld width and reinforcement height (excess metal of the weld bead). The

top point  $b_3$  and border points  $b_1$  and  $b_2$  of the weld bead are selected as the feature points, as shown in Fig. 4(d). Unfortunately, the weld groove has fully been filled, and the laser stripe is almost flat, so that the curvature extremum method cannot be used to extract feature points, particularly in the presence of the disturbances in weld images. Here, a feature extraction method is used based on statistical analysis of a sequence of frames. First, the stripe profiles are extracted in each frame. The stripe profiles in a sequence of frames are strongly correlated.

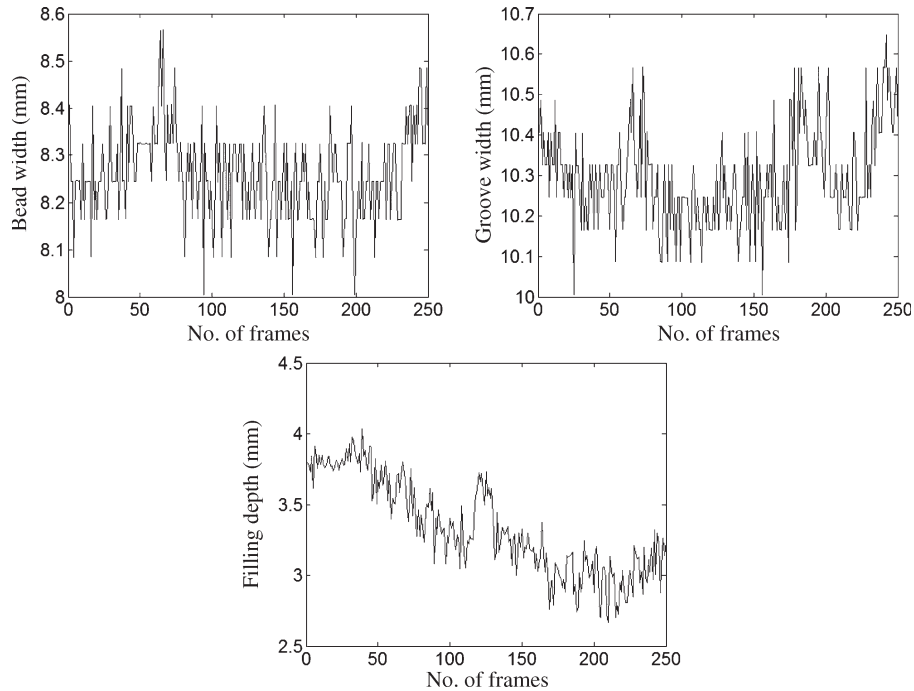


Fig. 8. Dimensional measurement for root-pass weld.

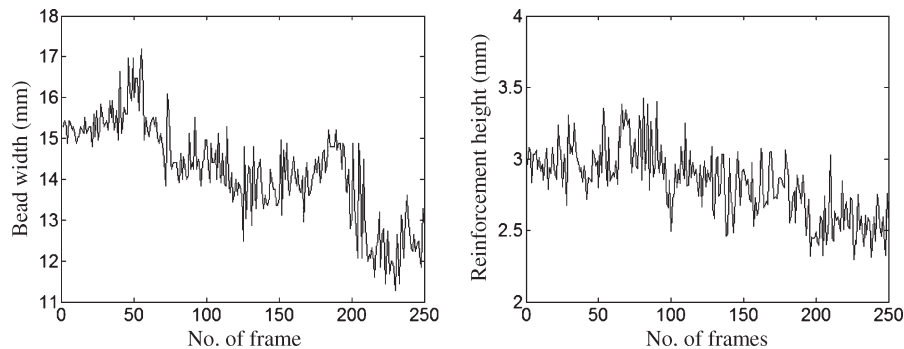


Fig. 9. Dimensional measurement for cap weld.

Thus, multiple-frame averaging is used to minimize zero-mean Gaussian noise. Then, a case deletion diagnostics is used to reject the false points on the profile, by which the points are divided into valid data and false points according to their influences on the fitting results. The cap weld bead dimensions can be calculated in the following manner: The baseline is detected using a Hough transform. The distance between corresponding points on the stripe profile and the baseline is calculated. Then,  $b_1$ ,  $b_2$ , and  $b_3$  are located based on the profile-to-base distance.

Reinforcement is the maximum height of the weld excess, and it can be calculated from the distance between the top point  $b_1$  of the weld bead and the baseline. Bead width is the distance between border points  $b_1$  and  $b_2$  on the bead profiles. In this paper, weld defects, including weld bead misalignment, plate displacement, and undercut, are concerned. During welding, weld bead misalignment occurs when the weld gun deviates from the weld seam, which can be detected by examining the lateral symmetry of the weld groove. Ideally, the feature points  $p_1$ ,  $p_2$ ,  $p_3$ , and  $p_4$  form an isosceles trapezoidal shape after root-pass weld. The shape would be deformed if bead misalignment occurred, i.e., the torch deviated from the weld seam. Plate

displacement is equal to the vertical distance between two baselines, which can be extracted from the Hough transform of the profiles. Undercut defects occur when the weld bead cuts the surface of the weldment. It can be detected by monitoring the distance between the two border points  $b_1$  and  $b_2$  and comparing it with the average groove width.

#### IV. EXPERIMENTAL RESULTS

Four experiments were conducted involving online inspection of the weld bead, including defect-free root-pass weld,

TABLE I  
AVERAGE DIMENSIONS OF THE WELD BEAD (IN MILLIMETERS)

	Vision measurement (N=250)		Mechanical measurement (N=10)	
	Root pass	Cap weld	Root pass	Cap weld
<i>Groove width</i>	10.3	N/A	10.6	N/A
<i>Bead width</i>	8.2	13.7	8.6	14.2
<i>Filling depth</i>	3.3	N/A	3.0	N/A
<i>Reinforcement</i>	N/A	2.9	N/A	2.6

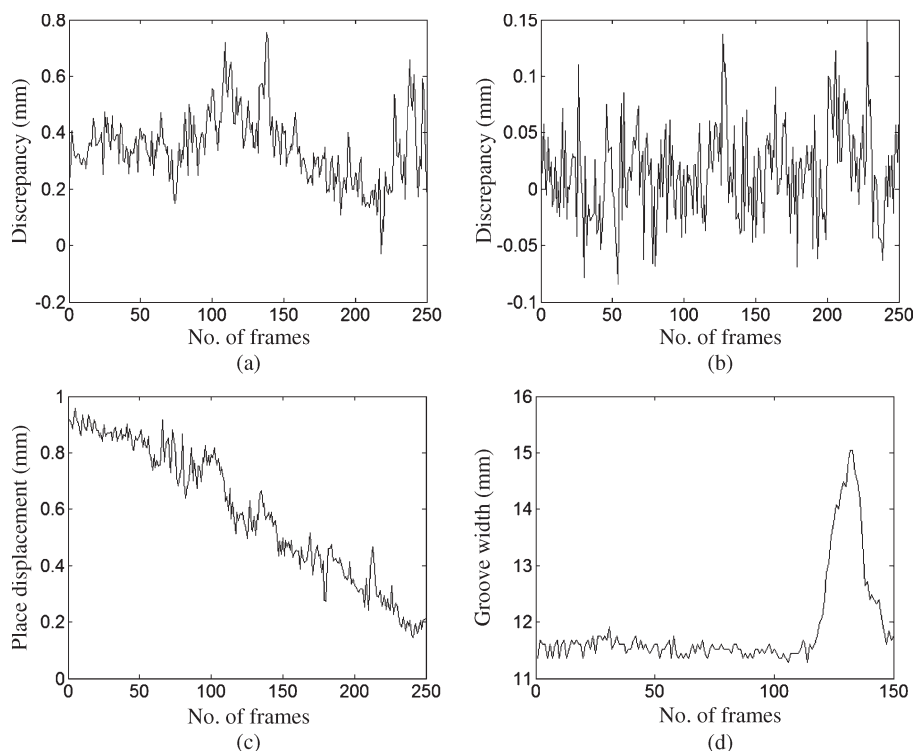


Fig. 10. Defect detection for misalignment, plate displacement, and undercut. (a) Misalignment defect. (b) Aligned weld bead. (c) Plate displacement trend. (d) Undercut defect.

defect-free cap weld, misalignment defect, and undercut defect. Four workpieces with a V-preparation joint were selected for gas-shielded multilayer welding. The welding parameters, such as voltages, currents, and the position of weld gun, were varied to obtain the ideal weld bead and weld defects for the inspection. Image processing, feature extraction, dimension measurement, and defect detection algorithms presented in this paper were tested.

Fig. 5 shows the profile and feature extraction of the laser stripe by the algorithms presented in Section III. The heavy reflection on a polished surface of the workpiece in Fig. 5(a) results an intensity profile in Fig. 5(b) as an example of typical signal noise. Fig. 5(c) shows that the stripe profile was extracted from the image despite the presence of glare and reflection. Fig. 5(d) shows the second derivative of Fig. 5(c), by which the feature points were extracted.

In the visual inspection system presented in this paper, the distance between the optical center of the camera and the weldment surface is approximately 100 mm, and the angle between the optical axis of the camera and the structured light plane is  $30^\circ$ . The scalar factors  $k_u$  and  $k_v$  of the inspection system are 0.08 and 0.14 mm/pix, respectively, and represent the horizontal and vertical resolutions of the system. The weld bead was scanned by the structured light sensor. A sequence of images was processed, and visual features were extracted. The photos and profiles of the weld beads in multilayer weld are shown in Figs. 6 and 7.

Fig. 6(b) and (d) shows the profiles of defect-free weld beads in root-pass and cap welding. For comparison, Fig. 7(b) shows the profiles of the weld bead in root-pass weld with a misalignment defect. The bead misalignment can be detected

by examining the lateral symmetry of the weld groove figure. Fig. 7(d) shows the profiles of weld beads in cap weld with an undercut defect. The dimensions of the weld bead were measured, and the weld defects were detected using the profiles.

In Fig. 8, bead width, groove width, and filling depth measurements were obtained from a sequence of frames in root-pass weld. Fig. 9 shows the bead width and reinforcement height of a cap weld bead.

The root-pass and cap weld variables can be transformed from pixel units to standard measurement units. Thus, the average dimensions of the weld bead can be obtained from the visual features within 250 frames. The results obtained from the vision inspection system were confirmed using a vernier caliper as a precise mechanical measurement tool by sampling the weld bead ten times at equal intervals. The average dimensions by vision and mechanism measurements are shown in Table I.

Fig. 10 shows the results of defect detection. For the misalignment defect, the center point of the filling weld bead deviated from the centerline of the weld seam by 0.3 mm on average, as shown in Fig. 10(a). For comparison, the errors in the aligned weld bead are mostly close to zero, as shown in Fig. 10(b). The misalignment defects were detected by comparing the average discrepancy in a sequence of frames to a threshold value. The plate displacement defects were detected by the distance between the two baselines. Fig. 10(c) shows that the displacement remains within the displacement tolerance limit of 1 mm. Undercut defects were detected by monitoring the distance between the two border points  $b_1$  and  $b_2$  compared with the average groove width. Fig. 10(d) shows the abrupt change in the distance between the border points in the presence of undercut defects.

TABLE II  
PERFORMANCE OF THE INSPECTION SYSTEM ( $N = 250$ )

	Horizontal	Vertical
Standard deviation	0.35mm	0.25mm
False positive rate	3.2%	N/A
False negative rate	5.6%	N/A

Table II shows the standard deviation of the inspection system, the false positive rate, and the false negative rate. The standard deviation was obtained in the horizontal and vertical directions, respectively, because horizontal and vertical resolutions of the inspection system are different. Misalignment and undercut defects are related to the horizontal coordinates of visual features. Plate displacement defect, which is related to the vertical coordinates, is detected with a tolerance of 1 mm in welding production. The main error sources in vision measurement are the sensor misalignment and the error in camera calibration.

## V. CONCLUSIONS

In this paper, a vision inspection system using structured light has been presented. Using the inspection system, the dimensions of the weld bead have been measured in root-pass and cap welding, and defect detection with the visual feature has been implemented. A detailed analysis on the sensor configuration has been presented. The vision inspection system can easily be calibrated in scales without requiring complicated 3-D reconstruction of the weldment. Experimental results show that the weld bead dimensions (groove width, weld bead width, filling depth, and reinforcement height) can automatically be measured with satisfactory results. Typical weld defects (plate displacement, weld bead misalignment, and undercut) were detected online.

Future work will focus on increasing the resolution of the vision sensor and extend the adaptability of the system to include other kinds of weld joints such as fillet weld, butt weld, and lap weld.

## ACKNOWLEDGMENT

The authors would like to thank the reviewers for their comments and suggestions and also G. S. Wang, Chinese Academy of Railway Science, for his help in giving technical instructions in welding.

## REFERENCES

- [1] H. Chen, J. Li, X. Zhang, and Z. Deng, "Application of visual servoing to an X-ray based welding inspection robot," in *Proc. Int. Conf. Control Autom.*, Budapest, Hungary, Jun. 27–29, 2005, vol. 2, pp. 977–982.
- [2] X. Zhang, J. Xu, and Y. Li, "The research of defect recognition for radiographic weld image based on fuzzy neural network," in *Proc. 5th World Congr. Intell. Control Autom.*, Jun. 15–19, 2004, vol. 3, pp. 2661–2665.
- [3] G. J. Schuster, S. R. Doctor, and L. J. Bond, "A system for high-resolution, nondestructive, ultrasonic imaging of weld grains," *IEEE Trans. Instrum. Meas.*, vol. 53, no. 6, pp. 1526–1532, Dec. 2004.
- [4] M. V. Predoi, C. C. Petre, M. Rousseau, and M. Billy, "Ultrasonic inspection of defects in welded plates and tubes," in *Proc. IEEE Ultrason. Symp.*, Oct. 5–8, 1997, vol. 1, pp. 845–848.

- [5] H. Ewald, "3-Dimensional magnetic leakage field sensor in nondestructive testing," in *Proc. 20th IEEE Instrum. Meas. Technol. Conf.*, May 20–22, 2003, vol. 2, pp. 1309–1311.
- [6] I. M. Dar, K. E. Newman, and G. Vachtsevanos, "On-line inspection of surface mount devices using vision and infrared sensors," in *Proc. AUTO-TESTCON*, 1995, pp. 376–384.
- [7] M. D. Valle, P. Gallina, and A. Gasparetto, "Mirror synthesis in a mechatronic system for superficial defect detection," *IEEE/ASME Trans. Mechatronics*, vol. 8, no. 3, pp. 309–317, Sep. 2003.
- [8] B. K. Wong, M. P. Elliott, and C. W. Rapley, "Automatic casting surface defect recognition and classification," in *Proc. IEE Colloq. Appl. Mach. Vis.*, May 24, 1995, pp. 10/1–10/5.
- [9] F. Sikström, M. Ericsson, P. Nylén, and A. Christiansson, "3D-scanning for weld distortion measuring," in *Proc. IEEE Int. Instrum. Meas. Technol. Conf.*, Apr. 24–27, 2006, pp. 2132–2137.
- [10] M. Norgia, M. Annoni, and C. Svelto, "Optical instrument for real-time ultrasonic welder inspection," in *Proc. IEEE Int. Instrum. Meas. Technol. Conf.*, May 12–15, 2008, pp. 1458–1461.
- [11] E. Carvalho, L. Molina, E. Freire, R. Freire, and B. Luciano, "Fillet weld identification for automatic inspection of spherical tanks," in *Proc. IEEE Int. Instrum. Meas. Technol. Conf.*, May 1–3, 2007, pp. 1–6.
- [12] G. E. Cook, R. J. Barnett, K. Andersen, J. F. Springfield, and A. M. Strauss, "Automated visual inspection and interpretation system for weld quality evaluation," in *Conf. Rec. IEEE IAS Annu. Meeting*, Oct. 8–12, 1995, vol. 2, pp. 1809–1816.
- [13] R. Kovacevic and Y. M. Zhang, "Online measurement of weld fusion state using weld pool image and neurofuzzy model," in *Proc. IEEE Int. Symp. Intell. Control*, Sep. 15–18, 1996, pp. 307–312.
- [14] J. Wu, J. S. Smith, and J. Lucas, "Weld bead placement system for multipass welding," *Proc. Inst. Elect. Eng.—Sci. Meas. Technol.*, vol. 143, no. 2, pp. 85–90, Mar. 1996.
- [15] R. A. White, J. S. Smith, and J. Lucas, "Vision-based gauge for online weld profile metrology," *Proc. Inst. Elect. Eng.—Sci. Meas. Technol.*, vol. 141, no. 6, pp. 521–526, Nov. 1994.
- [16] D. Xu, L. Wang, Z. Tu, and M. Tan, "Hybrid visual servoing control for robotic arc welding based on structured light vision," *Acta Automatica Sinica*, vol. 31, no. 4, pp. 596–605, Jul. 2005.
- [17] Z. Yan, D. Xu, and Y. Li, "A visual servoing system for the torch alignment to initial welding position," in *Intelligent Robotics and Applications—Part I*, vol. 5314. Berlin, Germany: Springer-Verlag, pp. 697–706.
- [18] Y. Li, Q. Wang, Y. Li, D. Xu, and M. Tan, "On-line visual measurement and inspection of weld bead using structured light," in *Proc. IEEE Int. Instrum. Meas. Technol. Conf.*, May 12–15, 2008, pp. 2038–2043.
- [19] Y. Li, Q. Wang, D. Xu, Z. Yan, and M. Tan, "Recent developments on welding image processing and features extraction," *J. Inst. Meas. Control*, vol. 40, no. 5, pp. 139–145, 2007.



**Yuan Li** (M'08) received the B.Sc. and M.Sc. degrees in electrical engineering from Dalian Jiaotong University, Dalian, China, in 1999 and 2002, respectively, and the Ph.D. degree in control science and engineering from the Chinese Academy of Sciences, Beijing, China, in 2006.

In 2006, he joined Beijing Institute of Technology, Beijing. He was a Senior Researcher Associate from September 2007 to January 2008 with the City University of Hong Kong, Kowloon, Hong Kong. His research interests include robotics and computer

vision, particularly visual measurement and control of robots.



**You Fu Li** (M'91–SM'01) received the B.Sc. and M.Sc. degrees in electrical engineering from Harbin Institute of Technology, Harbin, China, in 1982 and 1986, respectively, and the Ph.D. degree in robotics from Oxford University, Oxford, U.K., in 1993.

From 1993 to 1995, he was a Postdoctoral Researcher with the Department of Computer Science, University of Wales, Aberystwyth, U.K. In 1995, he joined the City University of Hong Kong, Kowloon, Hong Kong. His research interests include robot vision, visual tracking, robot sensing, and sensor-

based control.

Dr. Li is an Associate Editor of the IEEE TRANSACTIONS ON AUTOMATION SCIENCE AND ENGINEERING.



**Qing Lin Wang** received the B.Sc. degree in control science and engineering from Beijing Institute of Technology, Beijing, China, in 1983 and the Ph.D. degree in control science and engineering from the Chinese Academy of Sciences, Beijing, in 1999.

He is currently a Professor with Beijing Institute of Technology. His research interests include nonlinear control, complex system modeling, and optimization.



**Min Tan** received the B.Sc. degree in control science and engineering from Tsing Hua University, Beijing, China, in 1986 and the Ph.D. degree in control science and engineering from the Chinese Academy of Sciences, Beijing, in 1990.

He is currently a Professor with the Laboratory of Complex Systems and Intelligence Science, Institute of Automation, Chinese Academy of Sciences. His research interests include robotic control and intelligent control.



**De Xu** (M'05) received the B.Sc. and M.Sc. degrees from Shandong University of Technology, Jinan, China, in 1985 and 1990, respectively, and the Ph.D. degree from Zhejiang University, Hangzhou, China, in 2001, all in control science and engineering.

He is currently a Professor with the Laboratory of Complex Systems and Intelligence Science, Institute of Automation, Chinese Academy of Sciences, Beijing, China. His research interests include robotics and automation, particularly the control of robots such as visual control and intelligent control.